Effect of residual stress in Pb ($Zr_{0.52}Ti_{0.48}$) O_3 – $BiFeO_3$ multilayer cantilever structure

Shankar Dutta[1*], Ramjay Pal[1] and Ratnamala Chatterjee[2]

[1]*Solid State Physics Laboratory, DRDO, Lucknow Road, Timarpur, Delhi 110054, India*
[2]*Department of Physics, IIT Delhi, Hauz Khas, New Delhi 110016, India*

[*]Corresponding author

DOI: 10.5185/amlett.2018.6973
www.vbripress.com/aml

Abstract

This paper discussed about the integration issues of Pb ($Zr_{0.52}Ti_{0.48}$) O_3 – $BiFeO_3$ (PZT - BFO) multilayer thin film deposited on silicon substrate for possible application in future micro-electro-mechanical system (MEMS) devices. The PZT - BFO multilayer thin film is deposited on silicon wafer by sol-gel technique. The multilayer film is annealed at 650 °C in air for 60 min. The deposited multilayer film is found to be polycrystalline in nature. The PZT-BFO multilayer exhibited room temperature multiferroic properties (remnant polarization of 37 μC/ cm^2 and remnant magnetization of 3.1 emu / cm^3). To fabricate the PZT - BFO multiferroic cantilever structures, a two-mask process flow is developed. Etch rates of the PZT - BFO multilayer (180 nm/ min), ZrO_2 buffer layer (35 nm/ min) and SiO_2 layer (350 nm/ min) are optimized in CHF_3 plasma. The multiferroic cantilever structures are released by isotropic etching of silicon using SF_6 plasma. Bending and cracks are observed in the released cantilever structures due to the generation of residual stress in the multilayer thin film. Effect of residual stress on the PZT - BFO cantilever structure is also verified by simulation.

Keywords: Pb ($Zr_{0.52}Ti_{0.48}$) O_3, $BiFeO_3$, etching, cantilever, residual stress.

Introduction

Thin films of multiferroic materials, which exhibit ferroelectric and magnetic orders, have drawn considerable attentions in recent years [**1-3**]. Bismuth ferrite ($BiFeO_3$) is one such multiferroic material. However, due to its weak ferroelectric properties and large leakage current density, the application of $BiFeO_3$ (BFO) is seriously hindered [**1-5**].

To overcome these problems, some researchers also obtained high quality multiferroics by combining two or more ferroelectric/ multiferroic materials [**6-15**]. The combination of Pb ($Zr_{0.52}Ti_{0.48}$) O_3 (PZT) – $BiFeO_3$ (BFO) multilayer thin film is one of the most promising 'artificial multiferroic' and is found to possess superior dielectric and ferroelectric properties. Majority of previously published literatures discussed about the microstructure and multiferroic properties of the PZT - BFO the multilayer films [**6-11**]. Jo et al. [**10**] have reported a maximum dielectric constant of 400 (at 1 KHz) in F PZT/BFO multilayer thin film. Yan et al. [**6**] have found a maximum dielectric constant of 300 (at 100 Hz) in 5% PZT modified BFO thin film. Stancu et al. [**8**] have reported dielectric constant 250 for 3 layers (2PZT and 1BFO); 375–475 for 5 layers (3PZT and 2BFO); and 700 for 7 layers (4PZT and 3BFO) with maximum tunability of 17% at 5 V in the 5-layer structure. In our earlier communication we have reported about the 3 times improvement in remnant polarization due to the ZnO buffer layer compared to the multilayer thin film without buffer layer [**9**].

Integration of the PZT - BFO multilayer thin films on silicon wafers has tremendous importance especially for realization of variety of multiferroic based smart micro-electro-mechanical system (MEMS) devices. But there is still no reported literature on the deposition/ integration of PZT - BFO multilayer thin films with MEMS structures.

Most of the previously published reports related to the PZT-BFO multilayer discussed about its electrical properties measured across the film thickness applying bias between top and bottom electrodes [**6-11**]. Thus, ferroelectric and piezoelectric characteristics of the multilayer films are found to be dependent on its thickness. Many times it is difficult to deposit the films thicker than several micrometers without crack. An alternate to the above approach, one can think of measuring the electrical properties of PZT-BFO multilayer thin films deposited on any insulating substrate (without any bottom electrode) by creating inter-digitated terminal (IDT) structures on top of the film. Here, the electric filed lines tend to select ferroelectric medium compared to the air/surface leakage between the consecutive IDT [**16**]. The electric field lines is expected to be neither homogeneous in magnitude nor in direction [**16-17**]. However, if the finger gap is large compared to the film thickness, the vertical component of the electric field in the film beneath the electrode fingers is expected to be much smaller than the horizontal component of the

electric displacement between two fingers. In this condition the electric field lines between the adjacent electrode fingers are assumed to be homogeneous and parallel to the film's plane [**17**].

During the thin film deposition and its integration with any MEMS structure, residual stress is one of the most common after-effects [**18-21**]. It originates from misfits between different regions in the structure [**22-23**]. Domain of residual stresses can be expressed in terms of length over which the stresses equilibrate: *macroscopic stresses* which equilibrate over dimensions of the scale of the structure; and *microscopic stresses* which equilibrate over atomic dimensions and balance within a grain or even over a few number of grains [**23**]. Residual stress can enforce a variety of consequences, like deformation, fracture, fatigue etc. that may alter the behavior of the final MEMS device as well as its reliability [**18-21**].

In this paper, integration issues of PZT - BFO multilayer thin film with MEMS cantilever structure are highlighted. The PZT - BFO multilayer thin film is grown on silicon wafer by sol-gel technique. To fabricate multiferroic cantilever structures, a two-mask process flow is used. Etching of the PZT - BFO multilayer and ZrO_2 buffer layer are studied in CHF_3 plasma. Finally, the multiferroic cantilever structures are released by micromachining of silicon wafer using deep reactive ion etching (DRIE) system. Effect of residual stress on the PZT - BFO multilayer cantilever structure is also simulated using finite element method (FEM) based software. Dimensions of the multilayer cantilever structure are tabulated in **Table 1**.

Table 1. Dimensions of the PZT - BFO multilayer cantilever.

Parameters	Dimension (μm)
Cantilever length (L)	750
Cantilever width (w)	500
Silicon thickness (t_{si})	25
SiO_2 thickness (t_{SiO2})	0.8
ZrO_2 buffer layer thickness	0.04
PZT - BFO multilayer thickness ($T_{PZT - BFO}$)	0.2
Cr- Au thickness (t_M)	0.1

Experimental

Deposition of PZT - BFO multilayer on silicon

In this study, the sols of ZrO_2, $BiFeO_3$, and $Pb(ZrTi)O_3$ are synthesized using the metal alkoxides, metal acetates, metal nitrates, and 2-methoxyethanol. The 0.3 M ZrO_2 sol is prepared using zirconium-n-propoxide ($Zr[O(CH_2)_2CH_3]_4$; Alfa Aesar) as precursors dissolved in 2-metoxyethanol (Sigma Aldrich). The 0.3 M $Pb(ZrTi)O_3$ sol is produced by dissolving lead acetate tri-hydrate ($Pb(CH_3COO)_2$, $3H_2O$; Sigma Aldrich), zirconium n-propoxide, and titanium isopropoxide ($Ti[OCH(CH_3)_2]_4$; Alfa Aesar) in 2-methoxyethanol. The 0.3 M $BiFeO_3$ sol is synthesized by dissolving bismuth nitrate penta-hydrate ($Bi(NO_3)_3$, $5H_2O$) and Fe nitrate non-anhydrate ($Fe(NO_3)_3$, $9H_2O$; Alfa Aesar) in 2-methoxyethanol. The 10% molar excess Pb and 10% molar excess Bi are added in the PZT and BFO sols respectively to compensate Pb and Bi loss during the annealing at elevated temperature.

Prior to the deposition process the silicon wafers are cleaned in trichloroethylene acetone, and de-ionized water and subsequently dried. After this, the ZrO_2 buffer layer is spin-coated (KarlSuss-make spin-coater) on the silicon wafer at 5000 rpm for 45 s and then baked on a hot plate at 250 °C for 5 min. Then, the ZrO_2 film is annealed at 700 °C in a preheated tube furnace for 30 min in air. After depositing the ZrO_2 buffer layer, PZT sol is spun on the substrate at 5000 rpm for 45 sec and dried at 250 °C for 5 min. Then, BFO sol is spin coated and dried under the same conditions. This route is repeated several times to form the multilayer thin films of three layers of PZT and two layers of BFO. Finally, the film is annealed at 650 °C in a furnace for one hour. The phase and crystalline structure of the ZrO_2 buffer and PZT-BFO multilayer films are analyzed using a high-resolution X-ray diffraction (PANalytical PW 3050/65 X-Pert Pro MRD HRXRD). Multiferroic (ferroelectric and magnetic) behavior of the film is studied using a SQUID magnetometer (MPMS-XL) and PE Loop Tracer (Precision Premier II, Radiant Technologies, Albuquerque, NM, USA).

Cantilever fabrication process flow

For fabrication of the PZT - BFO multilayer cantilever structures, the mask layouts are designed in AutoCAD 2004 software. The first mask is used to define the inter digitated terminal (IDT) metal lines (Mask 1), and the second one is for the patterning of cantilever structure (Mask 2). In absence of bottom electrode, the IDT structures are created to measure the electrical properties of the multilayer film. To fabricate the cantilever structure wet chemical etching of silicon by using aqueous alkaline solutions (KOH, TMAH etc.) is tried. The PZT - BFO multilayer is washed away in the etching solutions. Finally the multiferroic cantilever structures are released by micromachining of silicon using deep reactive ion etching (DRIE). Detailed process sequences for the fabrication of the cantilever beam are discussed in **Fig. 1**.

First, Si (100) wafer is cleaned by the standard RCA cleaning procedure. The Si (100) wafer is thermally oxidized (dry – wet – dry) at 1150 ºC to grow oxide of thickness ~ 0.8 μm as shown in step (a). Then ZrO_2 buffer layer is deposited by using spin coating and subsequently annealed for crystallization. Thereafter, PZT - BFO multilayer thin film is deposited by multiple (3 layers PZT and 2 layers BFO) spin coating (step (b)). The window for IDT formation is defined by photolithography (Mask 1). Cr (30 nm)–Au (100 nm) layers are deposited by using vacuum evaporation system and IDT structures are formed by lift-off technique by photoresist stripping as shown in step (c). The cantilever structure is then defined by photolithography with precise alignment (Mask 2) as depicted in process step (d). The photoresist layer is used as masking layer to pattern the PZT - BFO multilayer, ZrO_2 buffer layer and SiO_2 layer.

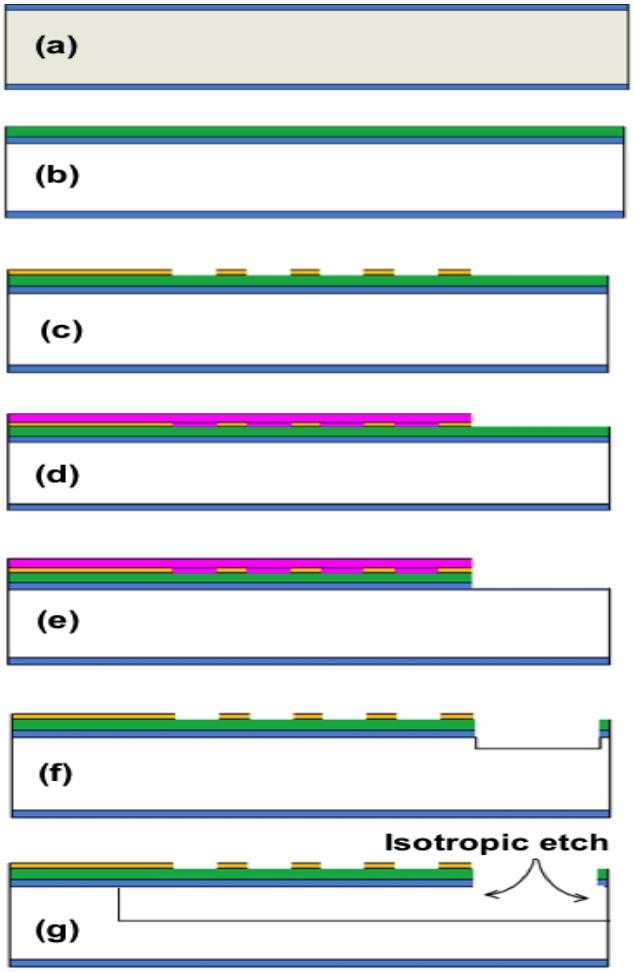

Fig. 1. Fabrication process flow for the multiferroic cantilever structure.

These layers are then patterned by deep reactive ion etching (DRIE) system (SPTS LPX Pegasus, MP0667) using CHF_3 (50 sccm) process gas as shown in step (e). Here, argon gas is used to initiate high-density inductively coupled plasma (ICP) plasma for the etching. Before the patterning, the etch rate of the PZT - BFO multilayer, ZrO_2 buffer layer and SiO_2 layer are optimized with ICP power (500 – 2500 W). Thereafter, the silicon layer is etched upto 25 μm depth (using the same DRIE equipment) is done at the exposed silicon wafer area as presented in process step (f). During the DRIE process, RF power and sequential etching-deposition cycles (Bosch process) of the dry etching process are optimized. In this etching process, SF_6, O_2, C_4F_8 gases are used. The SF_6 (flow rate: 330 sccm) and O_2 (flow rate: 33 sccm) gases are used during the etching cycle while C_4F_8 gas (flow rate: 150–200 sccm) is used in deposition cycle. Finally, the cantilever structure is then released by isotropic etching of the silicon wafer using DRIE as shown in step (g). During the isotropic etching the SF_6 and O_2 gases are continuously flowed while C_4F_8 gas flow is stopped. In all these dry etching experiments, platen temperature of the DRIE equipment is kept at 10 ºC to reduce the erosion of the masking layer (photoresist).

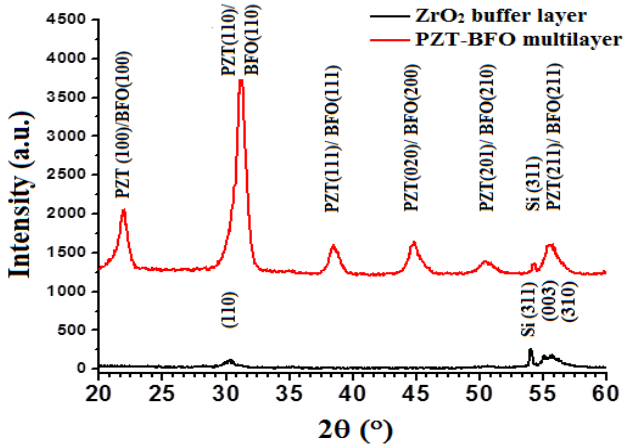

Fig. 2. XRD patterns of ZrO2 buffer and PZT-BFO multilayer structures.

Results and discussion

Discuss all the results and corresponding discussions in this section. Make sure a proper that proper coherency is maintained and appropriate discussions are included.

Phase and crystal structure of the ZrO_2 buffer and PZT-BFO multilayer are analyzed by using XRD pattern as shown in **Fig. 2**. The XRD peaks at 30° and 50° and multiple peaks around 55° proved monoclinic crystal structure of the ZrO_2 buffer layer deposited on the SiO_2/ Si sample is [**16**, **24**]. The multilayer exhibited phase pure polycrystalline perovskite structures of tetragonal PZT [**9, 16**] and rhombohedral BFO [**2-3**]. The XRD peak corresponding to the Si (311) plane observed around 55° contributed from silicon substrate.

Fig. 3 shows multiferroic properties (ferroelectric and magnetic) of the multilayer thin film. The film exhibited weak ferromagnetism at room temperature. The M-H loop in **Fig. 3** shows a remnant magnetization (M_r) of 3.1 emu/ cm^3 with a saturated magnetization (M_s) of 5.7 emu/ cm^3. The inter-diffusion of constituent elements of the PZT and BFO layers into each other seems to be the reasons for weak ferromagnetism in the multilayer compared to pristine BFO layers reported previously [**25-26**].

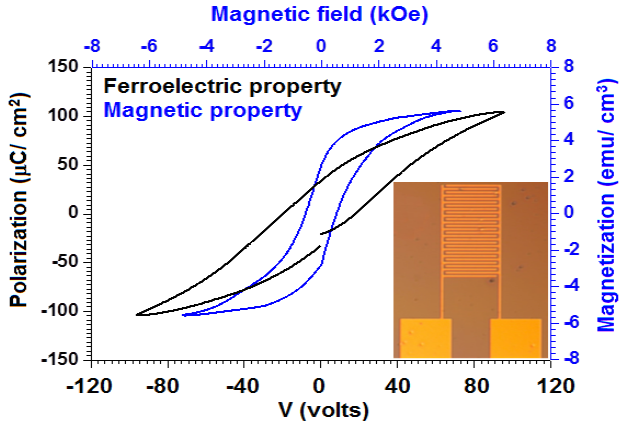

Fig. 3. Multiferroic properties (ferroelectric and magnetic hysteresis loops) of PZT-BFO multilayer. (Inset: fabricated Inter-digitated electrodes (Au) on the PZT - BFO multilayer).

The multilayer film showed characteristic ferroelectric hysteresis loop with a remnant polarization (P_r) of ~37 μC/ cm^2 at a 100 V bias as shown in **Fig. 3.** The IDT structures of Cr –Au layer are fabricated by lift-off technique as shown in inset of **Fig. 3**. The gap between the adjacent IDT lines is kept large enough (15 μm) in order to avoid shorting due to particle contamination during the ferroelectric measurement.

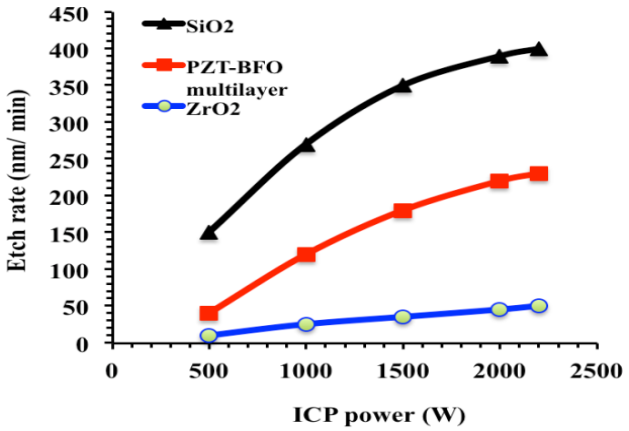

Fig. 4. Comparison of etch rates of PZT - BFO multilayer, ZrO_2 buffer layer and SiO_2 layer using CHF_3 plasma at 500 – 2500 W ICP power.

The etch rates of PZT - BFO multilayer, ZrO_2 buffer layer and SiO_2 layer using CHF_3 plasma are studied at 500 – 2500 W ICP power. **Fig. 4** shows the comparison of etch rates of the layers at different ICP power. The etch rates of the layers are found to increase with the increase in ICP power. However, with the increase in ICP power above 2000 W, the deterioration of photoresist masking layer is observed. Thus, for continuous etching of these layers at one-go, the ICP power is kept at 1500 W. At this ICP power, the optimized etch rate of the PZT - BFO multilayer, ZrO_2 buffer layer and SiO_2 layer are found to be 180 nm/min, 35 nm/ min and 350 nm/min respectively.

After the patterning of PZT - BFO, ZrO_2 and SiO_2 layers by dry etching using CHF_3, 25 μm of silicon is anisotropically etched by Bosch process using the same DRIE. Optimized RF powers for the etching and deposition cycles of dry etching experiment are found to be 2000 W and 1850 W respectively. Corresponding etching and deposition times for each cycle are 2.4 sec and 2 sec respectively. With this recipe, the problem of undercut is minimized and corresponding silicon etch rate is found to be ~ 4 μm/ min. **Fig. 5** shows SEM pictures of the patterned cantilever structure after etching the PZT - BFO, ZrO_2, SiO_2 and silicon layers.

Thereafter, PZT - BFO cantilevers structures are released by undercutting the silicon layer underneath the cantilever area using isotropic etching of silicon with continuous flow of SF_6 and O_2 gases at 2250 W etch power. Corresponding silicon isotropic etch rate is found to be ~ 7 μm/min. The released cantilever structure is shown in **Fig. 6**. **Fig. 6 (a)** shows the partially released cantilever structure during the silicon undercutting. After removing the underneath extra silicon, bending and crack generation is observed in the PZT - BFO multilayer cantilever structure as shown in **Fig. 6 (b)**. This bending and crack in the cantilevers seems to be due to the presence of residual stress in the multilayer thin film deposited on oxidized silicon.

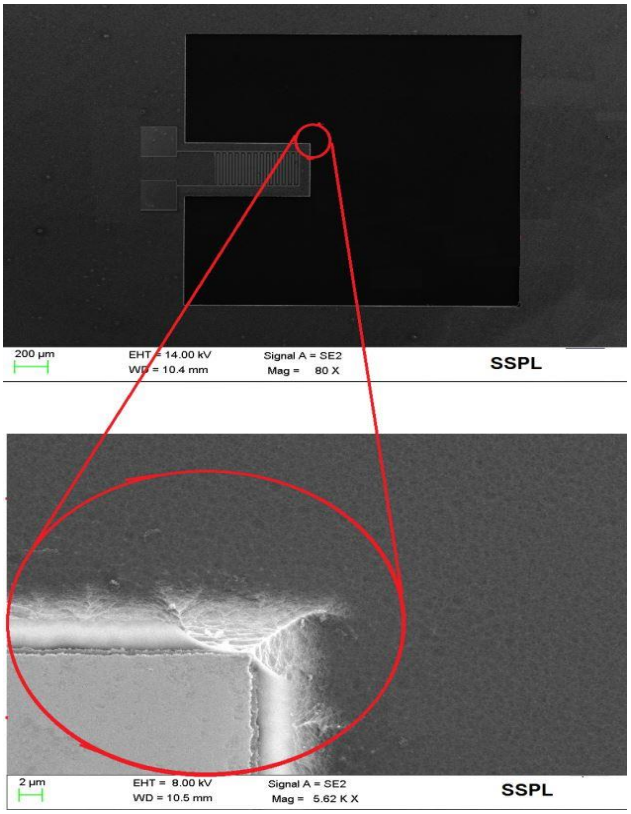

Fig. 5. Patterned the PZT - BFO multilayer ZrO_2 buffer and SiO_2 layers using CHF_3 plasma and silicon etched by using SF_6 and C_4F_8 based Bosch process.

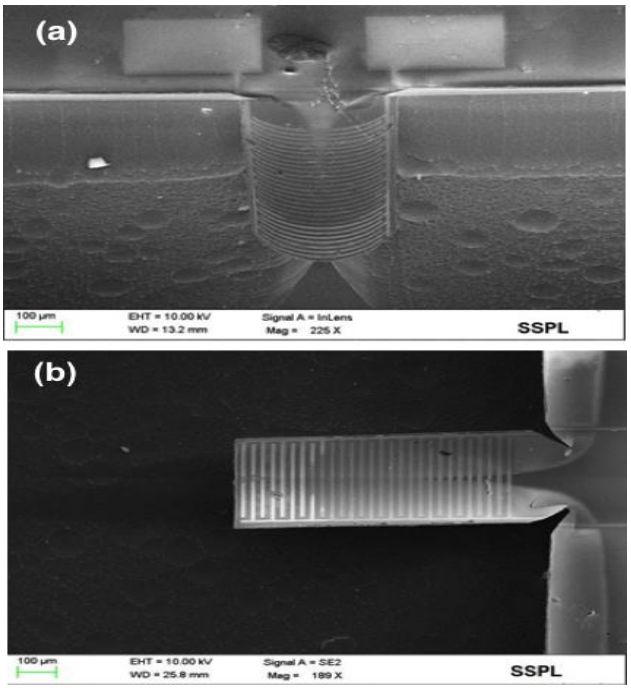

Fig. 6. Release of the PZT - BFO multilayer cantilever structure: (a) partially released cantilever and (b) fully released cantilever

In our earlier communication it was presented that the PZT-BFO multilayer thin film possesses residual stress which arises due to mismatches of thermo-elastic coefficients and/ or crystal lattice parameters of the multilayer film (PZT and BFO layers), buffer layer (ZrO_2) and substrate (Si) as well as due to constrained densification and shrinkage during annealing [**27-28**]. The residual stress in the PZT-BFO multilayer thin film was measured by x-ray diffraction and wafer curvature techniques respectively. Average residual stress in the multilayer film was found to be around 780 MPa (tensile) [**28**].

To analyze the effect of the residual stress on the cantilever structure, Finite Element Model (FEM) simulations are carried out using Coventorware™ 2012 software. During the FEM simulations, the residual stress value of PZT - BFO multilayers (780 MPa) is embedded in the cantilever structure. As cantilever structures are fixed at one end and free at the other end, bending of the cantilever is observed due to the residual stress. Simulation results of the cantilever structure are shown in **Fig. 7**. **Fig. 7 (a)** shows the simulated result of bending of the PZT - BFO cantilever beam due to the residual stress. The corresponding Von-misses stress contours are shown in **Fig. 7 (b).** The maximum Von-misses stress areas are most vulnerable of crack generation as highlighted (in red circles) in **Fig. 5 (b),** which is consistent with the cracks propagation as shown in **Fig. 6 (b).**

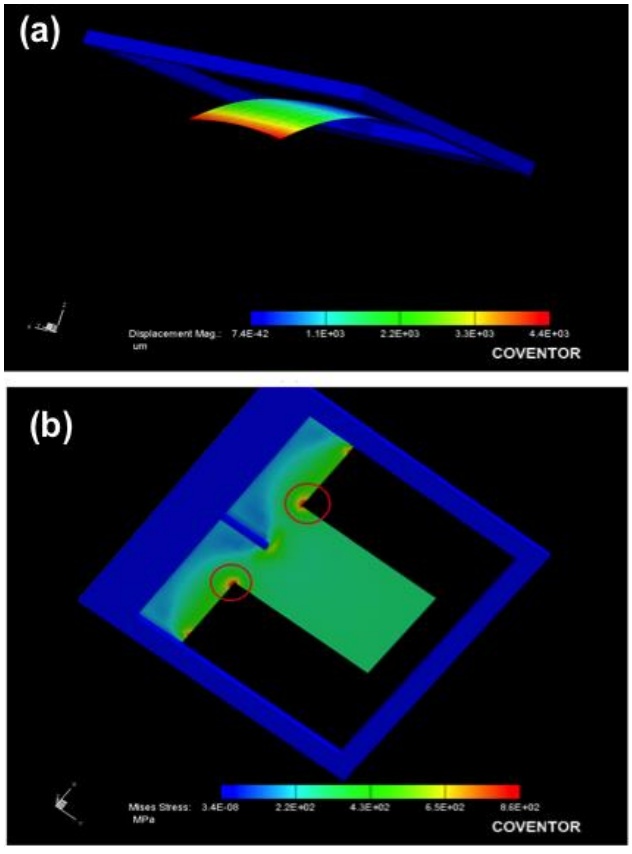

Fig. 7. Simulation results of the PZT - BFO cantilever structure under 780 MPa residual stress (a) deflection and (b) Von-misses stress contours.

Conclusion

In this paper, integration issues of PZT-BFO multilayer thin film with MEMS structure are highlighted. The PZT-BFO multilayer thin film is deposited on silicon wafer by sol-gel technique and subsequently annealed at 650 °C in air for 60 min. The deposited multilayer film is found to be polycrystalline in nature. The film showed room temperature multiferroic properties (ferroelectric and weak ferromagnetic). The film exhibited remnant polarization of 37 μC/ cm^2 at 100 V. The M-H measurement of the film showed a remnant magnetization of 3.1 emu/ cm^3. A two-mask process flow is designed to fabricate PZT - BFO multiferroic cantilever structures. The PZT - BFO multilayer, ZrO_2 buffer layer and SiO_2 layer are patterned using CHF_3 plasma. Optimized etching rates of the PZT - BFO multilayer, ZrO_2 buffer layer and SiO_2 layer are found to be 180 nm/ min, 35 nm/ min and 350 nm/ min at 1500 W ICP power respectively. The multiferroic cantilever structures are released by micromachining of silicon wafer using deep reactive ion etching (DRIE) system. Released cantilever structure showed bending and cracks generation due to the residual stress (780 MPa) in the multilayer thin film. The bending and crack propagation in the PZT - BFO multilayer cantilever structure due to the presence of residual stress is verified by FEM based simulation.

Acknowledgements

The authors acknowledge Director SSPL for his continuous support and for the permission to publish this work. Help from other colleagues are also acknowledged.

Author's contributions

Conceived the plan: SD and RC; Performed the expeirments: SD and RP; Data analysis: SD, RP and RC; Wrote the paper: SD, RP and RC. Authors have no competing financial interests.

References

1. Spaldin, N.A.; Cheong S.W.; Ramesh R.; *Physics Today*, **2010**, *63*, 38. **DOI:** 10.1063/1.3502547
2. Pradhan A.K.; Zhang K.; Hunter D.; Dadson J. B.; Loutts G. B.; Bhattacharya P.; Katiyar R.; Zhang J.; Sellmyer D. J.; Roy U. N.; Cui Y.; Burger A.; *J. Appl. Phys.*, **2005**, *97*, 093903. **DOI:** 10.1063/1.1881775
3. Singh S.K.; Kim Y.K.; Funakubo H.; Ishiwara H.; *Appl. Phy. Lett.*, **2006**, *88*, 162904. **DOI:** 10.1063/1.2196477
4. Yun K.Y.; Noda M.; Okuyama M.; Saeki H.; Tabata H.; Saito K.; *J. Appl. Phys.*, **2004**, *96*, 3399. **DOI:** 10.1063/1.1775045
5. Kumar A.; Yadav K.L.; *Mat. Sci. and Eng. B*, **2011**, *176*, 227. **DOI:** 10.1016/j.mseb.2010.11.012
6. Yan F.; Zhu T. J.; Lai M. O.; Lu L.; *J. Appl. Phys.*, **2011**, *110*, 114116. **DOI:** 10.1063/1.3668123
7. Wang N.; Cheng J.; Pyatakov A.; Zvezdin A. K.; Li J.; Cross L. E.; Viehland D.; *Phys. Rev. B*, **2005**, *72*, 104434. **DOI:** 10.1103/PhysRevB.72.104434
8. Stancu V.; Dragoi C.; Kuncser V.; Schinteie G.; Trupina L.; Vasile E.; Pintilie L.; *Thin Solid Films*, **2011**, *519*, 6269. **DOI:** 10.1016/j.tsf.2011.03.136
9. Dutta S.; Pandey A.; Yadav I.; Thakur O.P.; Laishram R.; Pal R.; Chatterjee R.; *J. Appl. Phys.*, **2012**, ***112,*** 084101. **DOI:** 10.1063/1.4759123

10. Jo S.H.; Lee S.G.; Lee Y.H.; *Nanoscale Res. Lett.* **2012**, *7*, 1. **DOI:** 10.1186/1556-276X-7-54
11. Kumari B.; Mandal P. R.; Nath T. K.; *Adv. Mat. Lett.* **2014**, 5, 84. **DOI:** 10.5185/amlett.2013.fdm.36
12. Murugavel P.; Singh M.P.; Prellier W.; Mercey B.; Simon C.; Raveau B.; *J. Appl. Phys.*, **2005**, *97*, 103914. **DOI:** 10.1063/1.1904153
13. Kaur M.; Yadav K. L.; Uniya P.; *Adv. Mater. Lett.* **2015**, 6, 895. **DOI:** 10.5185/amlett.2015.5861
14. Li J.; Li P.; Zhang G.; Yu J.; Wu Y.; Wen X.; *Thin Solid Films*, **2011**, *519*, 6021. **DOI:** 10.1016/j.tsf.2011.04.006
15. Layek S.; Verma H. C.; *Adv. Mat. Lett.* **2012**, 3, 533. **DOI:** 10.5185/amlett.2012.icnano.242
16. Dutta S.; Chatterjee R.; *Mat. Sci. Eng. B*, **2015**, *198*, 74. **DOI:** 10.1016/j.mseb.2015.03.013
17. Gevorgian S.S.; Martinsson T.; Linnkr P. L. J.; Kollberg E. L.; *IEEE Trans. MTT* **1996**, *44*, 896 **DOI:** 10.1109/22.506449
18. Sharmila M.; Kader S.M.A.; Ruth D.E.J.; Babu M.V.G.; Bagyalakshmi B.; Kumar R.T.A.; Padiyan D.P.; Sundarakannan B.; *Mat. Sci. Semicond. Process.*, **2015**, *34*, 109. **DOI:** 10.1016/j.mssp.2015.01.047
19. Dutta S.; Shaveta; Imran Md.; Pal R.; Bhan R. K.; *J. Mater Sci: Mater Electron.*, **2014**, *25*, 3828. **DOI:** 10.1007/s10854-014-2095-8
20. Dutta S.; Imran Md.; Pandey A.; Saha T.; Yadav I.; Pal R.; Jain K. K.; Chatterjee R.; *J. Mater Sci: Mater Electron.*, **2014**, *25*, 382. **DOI:** 10.1007/s10854-013-1598-z
21. Chinthakindi A.K.; Bhsari D.; Dusch B. P.; Musolf J.; Willemsen B. A.; Prophet E.; Roberson M.; Kohl P. A.; *J. Electrochem. Soc.*, **2002**, *149*, H139. **DOI:** 10.1149/1.1486454
22. Withers P. J.; Bhadeshia H. K. D. H.; *Mater. Sci. Technol.*, **2001**, *17*, 355. **DOI:** 10.1179/026708301101509980
23. Withers P. J.; Bhadeshia H. K. D. H.; *Mater. Sci. Technol.*, **2001**, *17*, 366. **DOI:** 10.1179/026708301101510087
24. Dutta S.; Pandey A.; Yadav I.; Thakur O. P.; Kumar A.; Pal R.; Chatterjee R.; *J. Appl. Phys.*, **2013**, *114*, 014105. **DOI:** 10.1063/1.4812733
25. Wang Y.; Nan C.W.; Appl. Phys. Lett., **2006**, *89*, 052903. **DOI:** 10.1063/1.2222242
26. Wang Y.; Nan C.W.; J. Appl. Phys., **2008**, *103*, 024103. **DOI:** 10.1063/1.2831026
27. Ong R. J.; Berfield T. A.; Sottos N. R.; Payne D. A.; *J. Eur. Ceram. Soc.*, **2005**, *25*, 2247. **DOI:** 10.1016/j.jeurceramsoc.2005.03.103
28. Dutta S.; Pandey A.; Thakur O. P.; Pal R.; Chatterjee R.; *J. Appl. Phys.*, **2013**, *114*, 174103. **DOI:** 10.1063/1.4828874

